Author/s:
Sui, X;Cox, D;Nie, S;Reid, GE;Hatters, DM

Title:
A Census of Hsp70-Mediated Proteome Solubility Changes upon Recovery from Heat Stress

Date:
2022-05-06

Citation:
Sui, X., Cox, D., Nie, S., Reid, G. E. & Hatters, D. M. (2022). A Census of Hsp70-Mediated Proteome Solubility Changes upon Recovery from Heat Stress. Journal of Proteome Research, 21 (5), pp.1251-1261. https://doi.org/10.1021/acs.jproteome.1c00920.

Persistent Link:
https://hdl.handle.net/11343/325364

Published manuscript doi: https://doi.org/10.1021/acs.jproteome.1c00920

# A census of Hsp70-mediated proteome solubility changes upon recovery from heat stress.

Xiaojing Sui[1], Dezerae Cox[2], Shuai Nie[3], Gavin E. Reid[2,4], Danny M. Hatters[2*]

[1]Department of Molecular Biosciences, Rice Institute for Biomedical Research, Northwestern University, Evanston, Illinois 60208, USA; [2]Department of Biochemistry and Pharmacology; and Bio21 Molecular Science and Biotechnology Institute, The University of Melbourne, VIC 3010. Australia; [3]Melbourne Mass Spectrometry and Proteomics Facility, Bio21 Molecular Science and Biotechnology Institute, The University of Melbourne, Parkville, VIC 3052, Australia; [4]School of Chemistry, The University of Melbourne, VIC 3010. Australia

*Correspondence: dhatters@unimelb.edu (D.M. Hatters). Twitter: @DannyHatters

**Abbreviations:** gene ontology (GO), liquid chromatography-nano electrospray ionization-tandem mass spectrometry (LC-nESI-MS/MS), false discovery rate (FDR), heat shock protein (HSP)

**ABSTRACT:** Eukaryotic cells respond to heat shock through several regulatory processes including upregulation of stress responsive chaperones and reversible shutdown of cellular activities through formation of protein assemblies. However, the underlying regulatory mechanisms of the recovery of these heat-induced protein assemblies remain largely elusive. Here, we measured the proteome abundance and solubility changes during recovery from heat shock in the mouse Neuro2a cell line. We found that prefoldins and translation machinery are rapidly down-regulated as the first step in the heat shock response. Analysis of proteome solubility reveals that a rapid mobilization of protein quality control machineries, along with changes in cellular energy metabolism, translational activity and actin cytoskeleton are fundamental to the early stress responses. In contrast, longer term adaptation to stress involves renewal of core cellular components. Inhibition of Hsp70 family, pivotal for the heat shock response, selectively and negatively affects the ribosomal machinery and delays the solubility recovery of many nuclear proteins. ProteomeXchange: PXD030069

**Keywords:** heat shock, chaperone, recovery, protein solubility, heat shock protein 70, disaggregation, quantitative proteomics

## INTRODUCTION

When a cell is subjected to a heat stress, the proteome becomes at risk of thermal denaturation and aggregation. To mitigate this, cells employ heat shock response mechanisms that involve the rapid transcription of stress-responsive chaperones (on the timescale of minutes), and subsequent translation over a timescale of minutes to hours[1-3]. The upregulation of chaperones increases the capacity for protein homeostasis to be restored quickly. While proteins may aggregate inappropriately when denatured, which may be detrimental to cellular health, recent evidence also indicates that protein assemblies can form as part of functional responses to restore proteostasis[4-6]. This includes RNA binding proteins that form condensates such as stress granules, which are thought to act by pausing normal processes that hinder the restoration of proteostasis, including translation and nucleocytoplasmic transport[4-6]. These condensates disassemble during the recovery from transient non-lethal heat stress[5, 6].

The heat shock protein 70 (Hsp70) family represents one of the core chaperone systems that governs the folding of nascent proteins and is pivotal to the heat shock response[7]. Under heat stress, one of Hsp70 family members, heat shock cognate 70 (Hsc70) shuttles from the cystosol into the nucleus to improve the folding of nuclear proteins[8, 9]. Hsc70 is also involved in the core of the protein disaggregase machinery, along with Hsp110 nucleotide exchange factor and J-protein co-chaperones of classes A and B in metazoans[10]. The disaggregases are efficient at dissociating functional aggregates as well as inappropriate aggregates formed by misfolded proteins, illustrating a broader role of Hsp70 in modulating protein assembly states[11]. Recent large-scale proteomics studies probed the recovery profile of proteome solubility from heat shock and revealed that ubiquitination is essential for recovery of cellular activities after heat shock in human cells[12, 13]. However, knowledge of which proteins in the proteome undergo assembly and disassembly upon a stress response recovery in mammalian cells, and which proteins are reliant on Hsp70, is only scantly understood.

Here, we sought to assess in a systematic manner how proteins in a mouse neuroblastoma cell line (Neuro2a) change solubility upon heat shock and how they recover over several hours, and to determine which proteins are most influenced by Hsp70 activity using a specific pan-Hsp70 family inhibitor (Ver155008)[14]. We apply "solubility" as an agnostic measure of a change in a protein's state of association with self or other proteins. We anticipate the solubility changes to reflect changes to proteins caused by heat denaturation and precipitation, and based on precedence[4-6], to reflect changes in protein binding patterns to other molecules as part of their functional response to the stimulus of heat shock (rather than precipitation due to denaturation). Our results indicate that proteome

remodeling after heat shock was directed primarily to upregulation of the protein disaggregation machinery and downregulation of protein translation machinery. Analysis of changes in proteome solubility revealed primary responses to heat shock, including rapid disassembly of machinery involved in ribosomes and their biogenesis, translation elongation, aerobic respiration, and nuclear-cytoplasmic transport; reduction of actin cytoskeleton and machinery involved in amino acid biosynthesis; and assembly of protein transport pathways, spliceosomes, and chaperone complexes. The longer term responses included assembly of structures involved in organelle synthesis. Hsp70 inhibition significantly down-regulated the ribosomal machinery and impeded the solubility recovery of many nuclear proteins.

## EXPERIMENTAL PROCEDURES

**Cell culture.** Neuro2a cells, obtained originally from the American Type Culture Collection (ATCC number: CCL-131), were maintained in Opti-MEM (Life Technologies) supplemented with 10% (v/v) fetal calf serum (Thermo Fisher Scientific), 1 mM glutamine, 100 U/mL penicillin and 100 µg/mL streptomycin (Life Technologies). $2.5 \times 10^6$ cells were seeded in 5 mL fresh media for 25 $cm^2$ plastic tissue culture flasks (Nunc EasYFlask (cat#nun156367)) and $6 \times 10^6$ in 10 mL media for 75 $cm^2$ flasks (cat# nun156472). Cells were grown for 18 hours before treatment in a humidified incubator with 5% (v/v) atmospheric $CO_2$ at 37 °C unless otherwise indicated. Cell count and viability were automatically determined using a Countess trypan blue assay (ThermoFisher Scientific).

**Heat stress, recovery and Hsp70 inhibition.** Heat shock was performed by replacing media on plated cells with fresh media pre-heated at 46 °C. Cells were then immediately kept in a humidified incubator with 5% (v/v) atmospheric $CO_2$ at 46 °C for the indicated time periods. After heat shock, the media was immediately replaced with fresh media, preheated at 37 °C, and cells were kept in a 37 °C incubator for the indicated recovery time periods before harvesting. For optimisation of the time period of heat shock, Neuro2a cells in 25 $cm^2$ flasks were heat shocked at 46 °C for 2, 4, 6, 8, 10, 15, 30, 45 or 60 min, followed by recovery at 37 °C for 1, 2 or 24 h. Cell viability was measured by trypan blue assay in samples collected after 1, 2 and 24 h recovery. As a second step to determine the heat shock conditions, Neuro2a cells in 25 $cm^2$ flasks were heat shocked at 46 °C for 5, 10 or 30 min, followed by recovery at 37 °C for 1, 2, 3, 5 or 24 h, and Hsp70 protein abundance was measured in samples collected after heat shock or 1, 2, 3, 5 and 24 h recovery by Western blotting. For proteomics analysis, Neuro2a cells were heated at 46 °C for 30 min, followed by recovery for 1, 2, 3 or 5 hours in 75 $cm^2$ flasks. For Hsp70 activity inhibition, cells were cultured in media supplemented with 20 µM Ver155008 (Sigma) for 18 hours

before heat shock. During heat shock and recovery, the corresponding fresh media were all supplemented with 20 μM Ver155008.

**Western blotting.** Cells were harvested by gently pipetting with phosphate buffered saline (PBS). Cells were pelleted by centrifugation at 120 g for 6 min and resuspended in 250 μL lysis buffer (2% SDS, 1% v/v IGEPAL-CA630, 50 mM Tris pH 7.4, 150 mM NaCl, 5 mM $MgCl_2$, 20 units/mL Benzonase (Millipore) supplemented with EDTA-free protease inhibitor (Roche)). Lysate was heated at 95 °C for 20 min. Debris was removed by centrifugation (13,000 rpm in a microcentrifuge; 10 min; 4 °C) and the supernatant placed in a new microcentrifuge tube. 10 μL cell lysates from each sample were loaded on an TGX Stain Free FastCast Acrylamide gel (BioRad, cat# 1610185). The amounts of total protein loaded in the gels were detected by UV light before gels were transferred using an iBlot2 gel transfer device (Thermofisher scientific, cat# IB21001) and a PVDF iBlot2 transfer stack (Thermofisher scientific, cat# IB24001). The membrane was blocked with 5% w/v skim milk powder in PBS for 1 h at room temperature. Anti-Hsp70 (Abcam, cat# ab5439) antibody was diluted to 1:1,000 in PBS containing 0.1% v/v Tween 20 and incubated overnight at 4°C. The secondary antibody, goat anti-mouse HRP antibody (Invitrogen, cat##31430), was diluted 1:10,000 in PBS containing 0.1% v/v Tween 20 and incubated for 1 hour at room temperature. HRP was detected by enhanced chemiluminescence kit (Clarity, BioRad).

**Cell fractionation by ultracentrifugation.** The separation of soluble and insoluble fractions was performed as previously described[15]. Briefly, Neuro2a cells were collected from the flasks with cell scrapers, followed by washing with phosphate buffered saline and pelleting at 120 g for 6 min for three times before being snap frozen in liquid nitrogen and kept at – 80 °C until use. Each cell pellet was resuspended in 500 μL ice-cold Buffer 1 (50 mM Tris-HCl, 150 mM NaCl, 1% (v/v) IGEPAL CA-630, 10 units/mL DNase I, 1:1,000 EDTA-free protease inhibitor tablet (Roche)) and lysed through a 27 G needle for 25 times, followed by a 31 G needle for 10 times. EDTA (0.5 M) was added to a final concentration of 2 mM. The cell lysate was split into two aliquots: a 300 μL aliquot and the rest left as being representative of the total (T) sample. The 300 μL aliquot was transferred to a chilled 1.5 mL ultracentrifuge tube and centrifuged at 100,000 g for 20 min at 4 °C. 250 μL of the resultant supernatant was reserved as the supernatant (S) sample. The T and S samples were resuspended in the same volume of Buffer 2 (Buffer 1, 4% (w/v) SDS, 4 mM DTT (1,4-dithiothreitol) ) as their initial volume, followed by incubation at 95 °C for 20 min. The concentration of proteins from T, S, and P fractions was measured by bicinchoninic acid assay by a dilution of 1:20 in PBS according to the manufacturer's instructions (Thermo Fisher Scientific).

**Sample preparation and TMT labeling for mass spectrometry.** 100 µg of protein from each sample was treated with 10 mM DTT for 1 h, followed by alkylation with 55 mM iodoacetamide for 1 h at 37 °C. Proteins were purified by chloroform/methanol precipitation (3). The resultant pellet was resuspended in 100 µL 8 M urea, 50 mM triethylammonium bicarbonate (TEAB) with vigorous vortexing. The solution was then adjusted to a final concentration of 1 M urea, 100 mM TEAB, followed by trypsin digestion (enzyme: protein mass ratio = 1:40) overnight at 37 °C. The peptides were desalted with a solid-phase extraction (SPE) cartridge (Oasis HLB 1 cc Vac Cartridge, 10 mg sorbent, Waters Corp., USA), followed by lyophilization by freeze drying (Virtis, SP Scientific) overnight. The pellets were resuspended in distilled water and quantified by bicinchoninic acid assay (Thermo Fisher Scientific) according to the manufacturer's instruction. 25 µg of each sample was labelled with TMT-11 plex isobaric labelling reagents (Thermo Fisher Scientific) following the manufacturer's instruction. Briefly, the TMT labeling reagents were equilibrated to room temperature immediately before use, then 41 µL of anhydrous acetonitrile was added to each tube of 0.8 mg TMT label reagent followed by intermittent vortexing over 5 minutes. The peptide solution was adjusted to pH 8 with 1 M TEAB, and the concentration of acetonitrile (ACN) adjusted to at least 30% (v/v). 4.1 µL TMT label reagent was then added to the corresponding peptide solution. The reaction was incubated at room temperature for 1 h with orbital shaking, followed by reaction quenching with the addition of 4 µL of 5% hydroxyl amine and incubation for 15 min. Equal amounts of TMT labelled peptides for different samples were then combined and lyophilized. The dried peptides were resuspended in 150 µL MS loading buffer (2% ACN, 0.05% trifluoroacetic acid (TFA) in water).

**Mass spectrometry analysis.** Samples were analysed by liquid chromatography-nano electrospray ionization-tandem mass spectrometry (LC-nESI-MS/MS). The nano-LC system, Ultimate 3000 RSLC (Thermo Fisher Scientific, San Jose, CA) was equipped with an Acclaim Pepmap nano-trap column (C18, 100 Å, 75 µm × 2 cm, Thermo Fisher Scientific, San Jose, CA) and an Acclaim Pepmap RSLC analytical column (C18, 100 Å, 75 µm × 50 cm, Thermo Fisher Scientific, San Jose, CA) maintained at a temperature of 50 °C. Typically, for each LC-MS/MS experiment 1 µg of the peptide mixture was loaded onto the enrichment (trap) column at an isocratic flow of 5 µL/min of 3% ACN containing 0.05% TFA for 5 min before the enrichment column was switched in-line with the analytical column. The eluents used for the LC were water containing 0.1% v/v formic acid and 5% v/v dimethyl sulfoxide (DMSO) for solvent A and acetonitrile containing 0.1% v/v formic acid and 5% DMSO for solvent B. The gradient used ( flow rate of 300 nL/min) was 3% B to 23% B over 144 min, 23% B to 45% B over 10 min, 45% B to 80% B over 10 min,

then maintained at 80% B for the final 5 min before dropping to 3% B over 1 min and equilibration for 8 min prior to the next analysis. The MS experiments were performed using a nESI source in positive ionization mode on a Fusion Lumos Orbitrap mass spectrometer (Thermo Fisher Scientific, San Jose, CA). The spray voltages, capillary temperature and S-lens RF level were set to 1.9 kV, 275 °C and 30%, respectively. The mass spectrometry data was acquired using a 3 second cycle time consisting of one full scan MS spectrum followed by as many data dependent HCD-MS/MS spectra as possible. Full scan MS spectra were acquired over an m/z range from 375-1500, a mass resolving power of 120,000 (at m/z 200), an auto gain control (AGC) target value of 4e5, and a maximum ion trapping time of 50 milliseconds. Data dependent HCD-MS/MS data acquisition was performed using an m/z isolation window of 0.7, for precursor ions with charge states from 2 to 7 a first mass at m/z of 100, a AGC target value of 1e5, a normalized collision energy (NCE) of 38%, and a maximum ion trapping time of 105 milliseconds. All MS/MS data were acquired using a mass resolving power of 50,000 (at m/z 200) in the Orbitrap mass analyzer. A dynamic exclusion time of 45 s was used.

**Proteomic data analysis.** Proteins were identified and quantified using Proteome Discoverer (version 2.3.0.81; Thermo Fisher Scientific) with the Mascot search engine (Matrix Science version 2.4.1). Data searches were conducted against the SwissProt *Mus Musculus* database (version 2015_07: Jun-24, 2015) with 16,724 proteins. For protein identification, the search was conducted with 20 ppm MS tolerance, 0.2 Da MS/MS tolerance and 2 missed cleavages with trypsin were allowed. Fixed modification was carbamidomethylation of cysteines. Variable modifications included methionine oxidation, and TMT labels on lysine and N-termini. The false discovery rate (FDR) was calculated by the Percolator node in Proteome Discoverer v 2.3.0.81, and accepted using values of 0.5% at the peptide level and 1% at the protein level. Proteins were filtered for those containing at least two unique peptides in all n=4 biological replicates from at least one condition group. The common contaminant, Keratin, was excluded from the dataset. Peptide quantitation was performed in Proteome Discoverer v.2.3.0.81 using the precursor ion quantifier node. The protein abundance in each replicate was calculated by summation of the unique peptide abundances used for quantitation. For total proteome analysis, the median protein ratio (i.e., stress/non-heat shock control) of each replicate was normalized to 1; for supernatant proteome, the median protein ratio (i.e., *pSup* = supernatant/total) of each replicate was normalized to 0.8 based on the proportion (~ 0.8) of the supernatant fraction out of the total lysate determined by the BCA assay. Solubility changes were calculated as $\Delta\ pSup = pSup_{\text{Non-heat shock control}} - pSup_{\text{Stress}}$. One- sample t-test (for ratios generated from the total proteome) and two-sample t-test (for *pSup* values generated

from the supernatant proteome) were performed to calculate the statistical significance with Perseus (v1.6.15.0). The ratios (R) from the total proteome and Δ *pSup* were scaled with a p-value weighted correction by the following two equations[16].

Equation 1 for calculating the p-value weighted ratio (*R**) for the total proteome:

$$R^* = 1 - \frac{1 - R}{-20^p}$$

where *R** corresponds to the mean of the total ratios and *p* corresponds to the p-value derived from one-sample t-test described above.

Equation 2 for calculating the p-value weighted ratio (Δ *pSup**) for the proteome solubility (*p* corresponds to the p-value derived from two-sample t-test described above):

$$\Delta\, pSup^* = \frac{\Delta\, pSup}{-20^p}$$

The resultant curves for Δ *pSup** during recovery from heat shock were clustered by K-means clustering using Weka 3.8[17]. The optimal number of clusters was determined manually to achieve minimal redundancy in clustered patterns.

**Bioinformatic analysis**. For Gene Ontology (GO) analysis, data were analyzed by the PANTHER overrepresentation test (PANTHER version 16.0, 20210224) using the PANTHER GO-Complete biological process, cellular component and molecular function datasets. Fisher's exact tests using FDR correction for multiple testing were performed. Results were filtered for GO terms containing at least four proteins, and a fold enrichment over 2 unless stated otherwise and *p* value less than 0.05. Protein interaction networks were generated using Cytoscape 3.7.1[18] with the built-in String (v11.0) tool[19] with a minimum required interaction score of 0.4 (medium confidence). For physicochemical properties analysis, Biopython[20] was used to calculate gravy score, isoelectric point, molecular weight, secondary structure prediction. IUPRed3 was used to calculate the percentage of intrinsically disordered proteins[21].

**Statistical analysis**. Statistical parameters are reported in the figures and corresponding figure legends. Figures were generated using the Seaborn package from Python v3. *P* values were considered significant at values less than 0.05 unless otherwise stated.

**Data availability.** The mass spectrometry proteomics data have been deposited in the ProteomeXchange Consortium database via the PRIDE[22] partner repository program with the dataset identifier PXD030069 (for whole proteome and solubility data). The information of the identified proteins are provided as the supplemental data.

## RESULTS & DISCUSSION

Two considerations were made in the approach to heat shock of Neuro2a cells. First was to ensure it was severe enough to induce the stress without compromising cell viability. Second was that the stress stimulated upregulation of the Hsp70 proteins. **Fig. 1A** shows that within 30 min of heat shock at 46 °C, cell viability was not affected. However, at heat shock lengths of 45 min or longer, cells detached from the flasks after 3 hours recovery, suggesting a compromise in viability. Heat stress for 30 min at 46 °C resulted in a more than 1.5-fold increase in Hsp70 abundance at 3 to 5 hours recovery, whereas heat shock for 10 min or less did not appear to induce Hsp70 upregulation (**Fig. 1B–D & Fig. S1**). This is consistent with the pioneer work in *Drosophila* that the total quantity of Hsp70 produced during heat shock and recovery is related to the severity of stress[23]. These results therefore indicated that a heat shock for 30 min at 46 °C was sufficient to induce the phenotype we sought without compromising cellular viability.

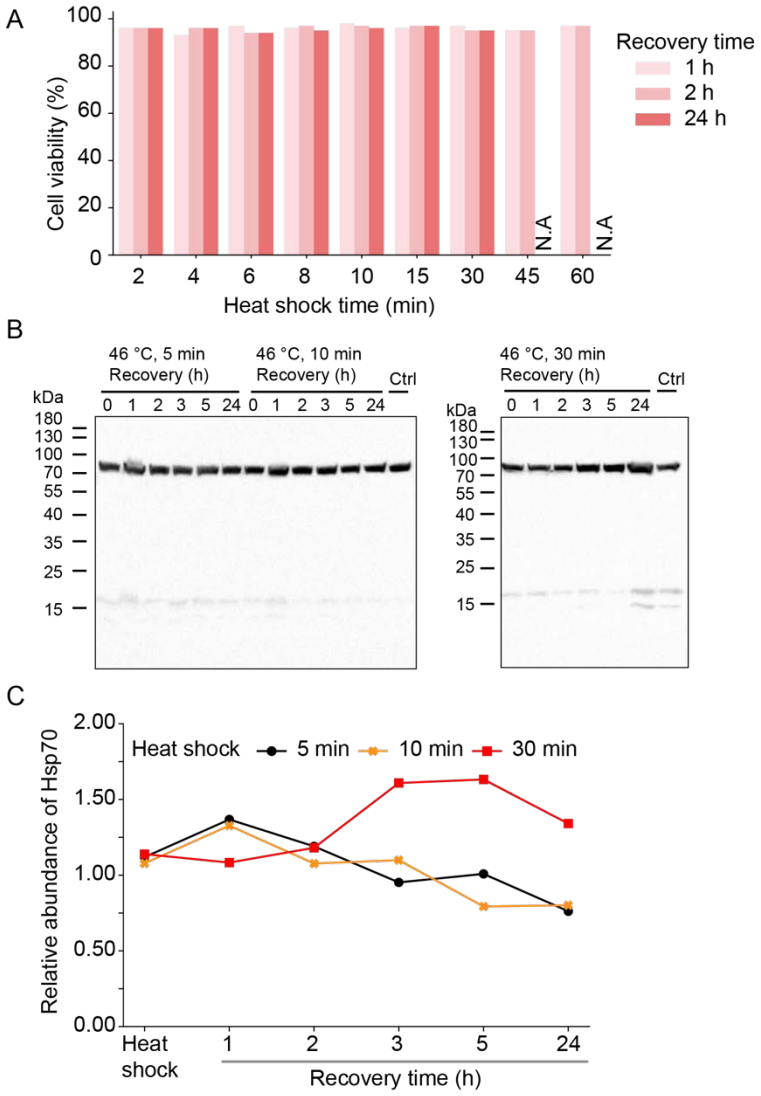


**Fig. 1 Optimization of the heat shock treatment.** (**A**). Neuro2a cell viability measured by trypan blue assay at the indicated time points of recovery from heat shock (46 °C). N.A. indicates samples where all cells had lifted from the plate and presumed dead. (**B**) Western Blots probed for Hsp70 for samples recovered at the indicated times (0, 1, 2, 3, 5 and 24 h) and heat shock treatment conditions (46 °C for 5, 10 or 30 min). The amount of total proteins per well is shown in Fig. S1. (**C)**. Quantitation of the immunoblot analysis shown in (B).

**Heat shock recovery involves downregulation of prefoldins and translational machinery and upregulation of Hsp70 chaperones involved in disaggregation.**

Tandem mass tag (TMT)-based multiplex quantitative proteomics was then used to monitor the abundances of individual proteins in samples collected over the heat shock and recovery time periods. An outline of the approach is shown in **Fig. 2A**. 3,042 proteins were identified in at least two replicates of all groups. We used a recently described statistical p-value-based smoothing approach to aid in identification of proteins that showed a significantly changed response[16]. This smoothing method weighs

the magnitude of the observed changes to the measured p-value so that meaningful changes are preserved whereas non-significant changes are suppressed to baseline. However, because the method adjusts the magnitude of responses, the reported magnitudes will be lower than the actual magnitudes (we report these adjusted fold changes or magnitudes as *; the uncorrected data for all data in the manuscript is shown in **Fig. S6**). This analysis yielded 19 proteins (0.58%) that changed abundance by at least 2-fold* at one or more timepoints after heat shock (**Fig. 2B, Table S1**). Of these, seven increased in abundance, including the Hsp70 co-chaperone Dnajb1. However, these proteins were not enriched in any functional groups by Gene Ontology (GO) analysis. Twelve proteins showed decreased abundances and were enriched in GO terms of ribosomal subunits (GO:0044391) and small molecule metabolic process (GO:0044281) (**Fig. 2C).**

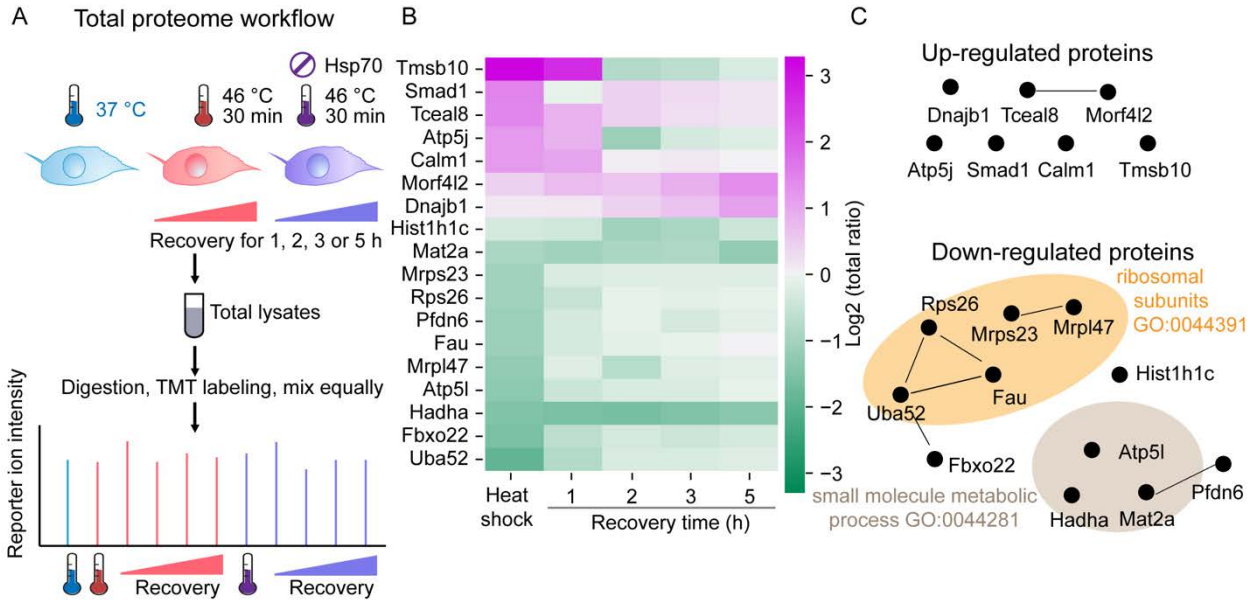


**Fig. 2. Total proteome abundance changes in Neuro2a cells after heat shock and during recovery.** (**A**) Schematic of the TMT-based quantitative proteomic workflow for measuring the total protein abundance changes after heat shock and during recovery. Treatment groups are shown. Hsp70 inhibition was achieved with 20 μM Ver-155008 added to the media 18 h before the heat shock. After heat treatment, media was refreshed and cells recovered for the indicated times before lysis with SDS-based buffers. Cells without heat shock, and Hsp70 inhibition were used as controls. The denatured cell lysates were reduced, alkylated, and desalted prior to protein digestionusing trypsin. After clean-up, peptides were labeled with TMT-11 plex, mixed equally and subjected to LC-MS/MS. Four biological replicates were used. (**B**) Heat map of proteins with significant relative abundance changes* ($P < 0.05$, above 2-fold change) in at least one timepoint after heat shock and during recovery. Purple represents increases and green represents decreases in abundance compared with pre-heat shock. (**C**) Protein networks of up-regulated or down-regulated proteins after heat shock or during recovery represented by STRING (v.11.0) analysis with medium confidence interactions. Selected significantly enriched gene ontology (GO) terms (above 2-fold enrichment and $P < 0.05$ from Fisher's exact test with FDR correction) are annotated.

A number of chaperones had abundance increases, including components of the protein disaggregase machinery[10] (Dnajb1, 2.18-fold*, Hspa8 (Hsc70) with 1.25-fold* and Hsph1 with 1.24-fold* at 5 h recovery) (**Fig. 3**). Unique peptides of other individual stress-inducible Hsp70s were not identified because these proteins are highly similar in sequence. However, we observed peptides in common to Hspa8 and Hspa1a/Hspa1b that were 1.8-fold* upregulated after heat shock and remained higher than 1.3-fold* at the recovery time points (**Fig. S2**). Small heat shock protein Hspb8, which is involved in preventing aggregation[24], also increased in abundance (1.3-fold*). In contrast, Hsp90- and Hsp60 family proteins showed limited changes in abundance (**Fig. 3**). Five out of six identified prefoldins, which are responsible for assisting the folding of newly synthesized proteins[25], were significantly down-regulated after heat shock (with 0.4 – 0.8-fold* decrease). In addition, 8 out of 45 identified large ribosomal subunits, particularly Rpl40, and 4 out of 31 small ribosome subunits were significantly down-regulated (by between 0.2 to 0.8-fold* decrease), while the rest identified subunits did not show significant changes (**Fig. S3A-B, Table S1**). These findings are consistent with an immediate degradation of machinery associated with translation and translation quality control upon heat shock as part of the first steps of the heat shock response. Both ribosome and prefoldin subunits returned to pre-heat shock abundances after 2 hours recovery (**Fig. 3 & S3A-B**).

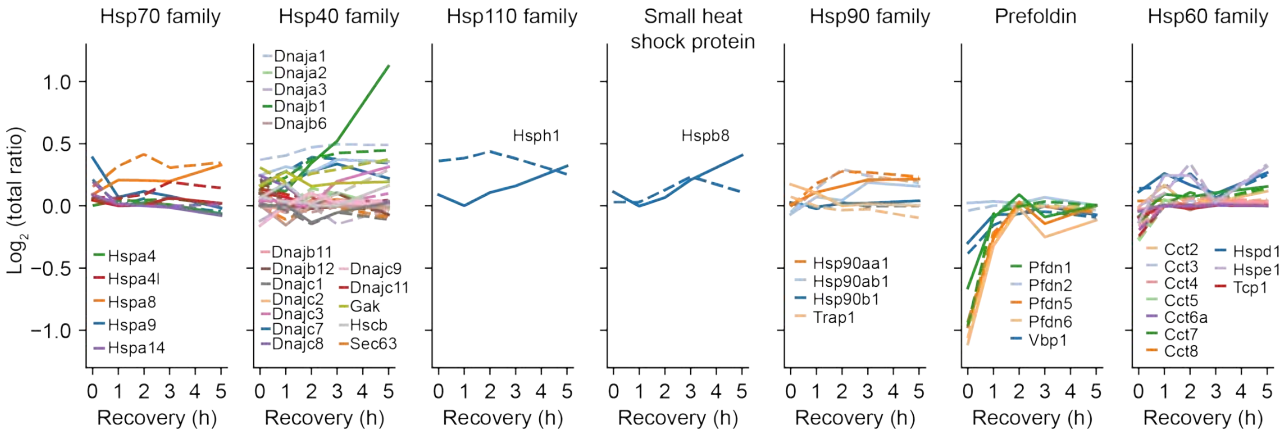


**Fig. 3. Abundance profiles of proteostasis network components after heat shock with or without Hsp70 inhibition.** Shown are fold changes relative to pre-heat shock after adjustment with p-value method (i.e. the approach suppresses statistically low confidence changes from zero). Solid lines indicate changes occuring after heat shock. Dashed lines indicate changes occuring with Hsp70 inhibitor added. Data are grouped by family type.

Other major changes in abundances due to heat shock included the mitochondrial ribosome. Nine out of 51 identified mitochondrial ribosomal proteins decreased abundance after heat shock (between 0.2 –

0.55-fold*), while the rest subunits did not change significantly (**Fig. S3C, Table S1**). Heat shock also decreased proteasome subunits (e.g. Psme4) modestly (**Fig S3D, Table S1**).

**Heat shock leads to selective changes in solubility of machineries involved in targeted cellular responses.**

Next we focused on proteome solubility changes, which can provide information on the protein networks that are remodeled [15]. For this we determined the *pSup* of individual proteins during heat shock recovery, which is the proportion of protein in the supernatant after a pelleting step (**Fig. 4A, Fig. S4**). 1,993 unique proteins were detected and measured across every time point of heat shock and recovery. Changes in the proportion of protein in the supernatant between control and treatment (Δ *pSup*) revealed widespread proteome solubility changes after heat shock, followed by restoration to baseline conditions upon recovery (**Fig. 4B, Table S2**).

A detailed examination of the kinetics of solubility changes of individual proteins was undertaken by a k-means clustering approach into 6 major groupings of kinetic patterns (**Fig. 4C, Table S3**). Of these clusters, four contrasting patterns were apparent. One involved proteins that underwent no major change in solubility (cluster 1 - 924 proteins, representing 46.3% of the identified proteome). Two clusters showed transient increases in solubility which differed in their magnitude* and extent of recovery (clusters 2 and 3; 508 proteins (25.5%) and 136 proteins (6.8%) respectively). Two clusters showed transient decreases in solubility which differed in their magnitude* and extent of recovery (clusters 4 and 5; 188 proteins (9.4%) and 68 proteins (3.4%). Finally, one cluster (Cluster 6, representing 169 proteins (8.5% of the proteome)), showed a progressive increase in insolubility* throughout the recovery time course, suggesting proteins changed aggregation state over a longer term and in a sustained manner.

To assess the biological mechanisms that align with these cluster patterns, we assessed the proteins in the above groups that underwent solubility changes by GO analysis (**Fig. 4D**). Clusters 2 and 3, whose members underwent increases in protein solubility, were associated with GO terms that illuminated the structural rearrangements that occur in the immediate aftermath of heat shock. GO terms enriched in biological processes included protein folding (GO:0006457), translation initiation (GO:0006413), positive regulation of establishment of protein localization to telomere (GO:1904851), protein deneddylation (GO:0000338), lysosomal protein catabolic process (GO:1905146), cell redox homeostasis (GO:0045454), tricarboxylic acid cycle (GO:0006099), establishment of mitochondrion localization, microtubule-

mediated (GO:0034643), pyruvate metabolic process (GO:0006090), regulation of actin filament depolymerization (GO:0030834), ATP metabolic process (GO:0046034), nucleotide biosynthetic process (GO:0009165), translational elongation (GO:0006414) and ribosome assembly (GO:0042255). Collectively these GO terms indicate a rapid mobilization of protein quality control machineries, changes in cellular energy metabolism, translational activity, and the actin cytoskeleton, and that remodeling of nucleotide biosynthetic processes are fundamental to the early stress responses. All of these changes result in a net reduction in the protein-protein interactions involved in their function.

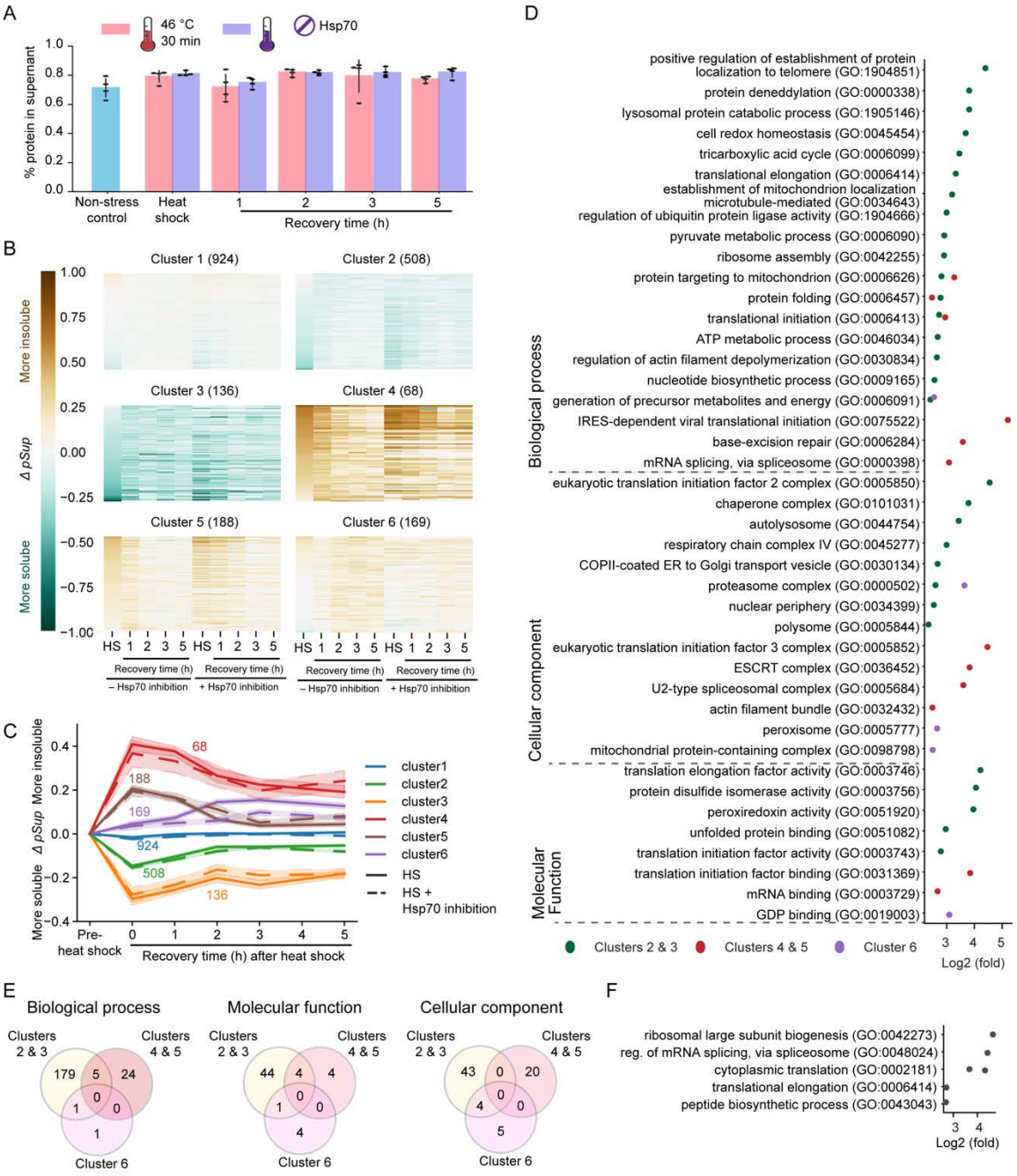


**Fig. 4. Proteome solubility changes in Neuro2a cells after heat shock and Hsp70 inhibition.** (**A**) Shown is the proportion of protein in the supernatant after lysis in nonidet-based buffers. Protein concentrations were measured by bicinchoninic acid assay. Means shown ± SD. N = 4. (**B**) Heat map showing solubility changes* (Δ *pSup*) after heat shock and during recovery of a total of 1993 proteins in the form of 6 clusters catergorized by K-means clustering. The number of proteins in each cluster were annotated. (**C**) K-means clustering of the solubility profiles* after heat shock and during recovery. Data shows means (lines) and 95% CI (shaded region) for the proteins in the cluster. The number of proteins in each cluster are annotated. (**D**) Selected significantly enriched GO Complete biological process, cellular component and molecular function terms for proteins in each cluster. (**E**) The common GO terms between clusters. (**F**) Significantly enriched GO terms in proteins that were specifically

affected by Hsp70 inhibition. GO terms with above 5-fold enrichment and $P < 0.05$ from Fisher's exact test with FDR correction were listed in **Table S4**.

Conversely, proteins in clusters 4 and 5, which showed increases in insolubility, revealed GO term enrichment for IRES-dependent viral translational initiation (GO:0075522), translational initiation (GO:0006413), protein folding (GO:0006457) and mRNA splicing, via spliceosome (GO:0000398). These patterns evoke formation of RNA splicing factor-enriched stress granules, activation of large-scale transport mechanisms, assembly of other complexes, which may include chaperone-based disaggregase complex formation.

Another point of note was that some GO terms contained proteins that showed opposite patterns of solubility change after heat shock, in that some lost and others gained solubility. These included translation initiation (GO:0006413) and protein folding (GO:0006457). Proteins in the translation initiation GO term that became more insoluble are drivers in IRES-dependent viral translation initiation (i.e. Csde1, Eif3d, Eif3b, Eif3f and pcbp2)[26, 27]. IRES-dependent viral translation initiation has been suggested to be involved in translating stress responsive mRNA under stress or viral infection[26, 27]. The increased insolubility of these proteins after heat shock may be explained by the formation of IRES-dependent translation initiation complex upon heat shock. In contrast, proteins involved in global translation initiation became more soluble after heat shock, suggesting the translation initiation complex is disassembled after heat shock to reduce global translation. Chaperones involved in protein folding were also divergent in their solubility changes (**Fig. 5**), suggesting different roles in responding to challenges of protein folding after heat shock. Ribosome-associated chaperone Hspa14 (a Hsp70 family member) and its co-chaperone, Dnajc2, became transiently more insoluble after heat shock, suggesting they may be sequestered into the aggregates formed by newly synthesized proteins vulnerable to heat shock[28]. Other Hsp70-, Hsp90- and Hsp110- family proteins became more soluble after heat shock suggesting they play different functions. Of the Hsp60 family, two members stood out from the others: Hspd1 and its co-chaperone Hspe1. These chaperones are distinct to other Hsp60 proteins by being localized to the mitochondria[29], suggesting a specific mitochondrial response. Prefoldin complex proteins also showed heterogenous changes in solubility. Three members showed transient increases in solubility after heat shock, Pfdn1 and Pfdn 6, which are β subunits of the prefoldin complex and the α subunit Pfdn5. Prefoldin 1, 5 and 6 were also down-regulated after heat shock (**Fig 3**), indicating that the instability of the prefoldin complex may lead to the removal of their subunits.

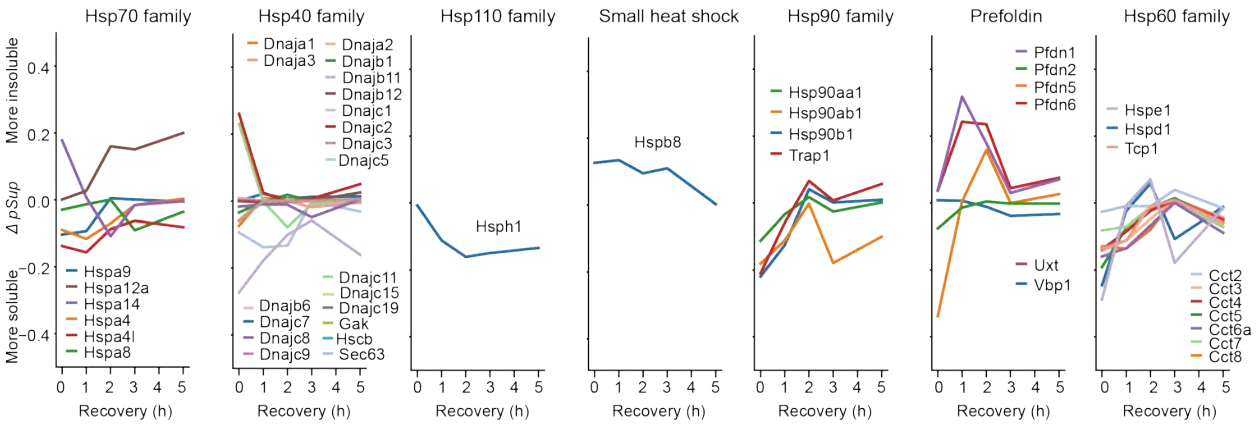


**Fig. 5. Solubility profiles of chaperones after heat shock and during recovery.** Shown are changes in solubility (relative to pre-heat shock; Δ *pSup*) after adjustment with p-value method (i.e. lines only indicate significant changes away from zero). Data is grouped by family type.

Proteins in Cluster 6, which shows progressive increases in solubility after heat shock and recovery, were enriched in positive regulation of proteasome complex (GO:0000502), mitochondrial protein-containing complex (GO:0098798), peroxisome (GO:0005777), positive regulation of cellular component biogenesis (GO:0044089) and positive regulation of cytoskeleton organization (GO:0051495). This finding is consistent with a longer-term adaptation to stress involving renewal of core cellular components.

**The heat-sensitive aggregation of proteins is not defined by protein folding stability**

Thus far our data points to many proteins that map strongly onto the biological pathways anticipated to be involved in the heat shock response and protein quality control. Next we examined whether there were also features of solubility change that points to underlying proteome thermostability which we predict would also relate to changes in aggregation. For this analysis, we obtained previously determined thermostability data[30] that was derived from apparent melting temperatures of proteins measured by their aggregation at different temperatures (in cell lysates). This published dataset included 1564 proteins that corresponded to our dataset. However, the proteins that changed solubility after heat shock did not correlate with their thermal stabilities (**Fig. 6A, Table S5**). Similarly, based on an analysis of protein folding stability data determined by methionine oxidation and urea denaturation curves[31], we found no correlation between the protein solubility changes resulting from heat shock and folding stability (**Fig. 6B, Table S5**). Next, we tested whether the protein solubility changes were biased toward protein total abundance changes in our own datasets (**Fig. 6C, Table S5**). The analysis also showed very poor correlation. Finally, we compared the physicochemical properties between soluble

proteins and aggregators upon heat shock (**Fig. S5**). We found that aggregators were enriched in proteins of high molecular weight, low isoelectric point, containing β-sheet and intrinsically disordered structure. These findings are in agreement with the findings previously reported in a different cell line after heat shock[12]. Collectively, these data suggest that the strongest driver of changes in proteome solubility related to rewiring of protein networks as a functional response to heat shock, which might be regulated by instrinscally disordered proteins, rather than heat-induced changes to aggregation arising from protein folding stability or abundances.

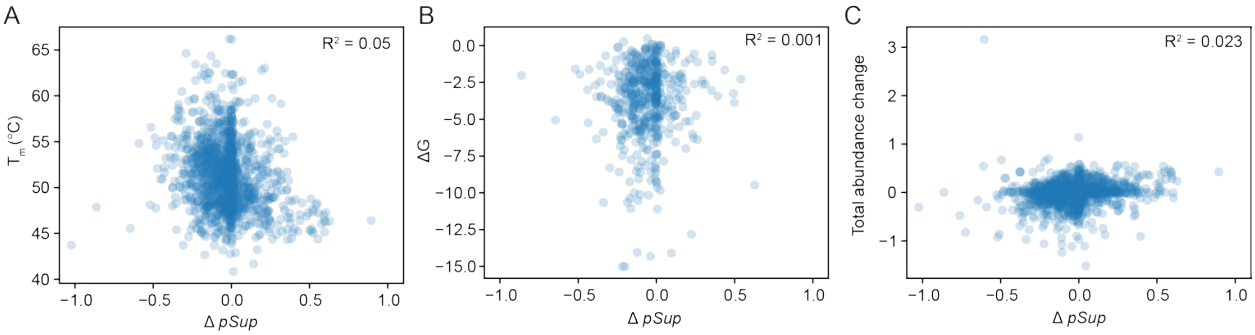


**Fig. 6. Proteins with solubility changes upon heat shock are not defined by thermal stability, folding stability, or protein abundance changes.** Correlation analysis of proteins that changed their solubility* upon heat shock with melting temperature[30] (**A**), free energy[31] (**B**) and total protein abundance (our data herein) (**C**).

**Hsp70 inhibition impedes the recovery of proteome solubility from heat shock**

Given the central role of the Hsp70 family proteins in responding to heat shock, we examined the impact when Hsp70 proteins were inhibited with the specific inhibitor Ver155008, which binds to the ATPase domain of Hsp70 family proteins with an $IC_{50}$ of 0.5 μM[14, 32]. First, we analyzed changes in total protein abundances mediated by Ver155008. Hsp70 inhibition dampened the up-regulation of Dnajb1 during the recovery from heat shock (**Fig. 3**) and significantly further down-regulated cytosolic large ribosomal proteins at all timepoints of recovery and the cytosolic small ribosome at a lesser extent (**Fig. S3A–B**). Treatment with Hsp70 inhibition did not further down-regulate the proteasome proteins (**Fig. S3D**). Hence, the Hsp70 machinery appears important to regulate the restoration of these immediate changes involving translation and translation quality control to baseline conditions and this may occur in both the general cellular translation machinery and the corresponding machinery of the mitochondria.

To identify key changes in how Ver155008 affects proteome solubility, we analyzed the solubility profiles of the above clusters with Hsp70 inhibition. In the k-means clusters, Hsp70 inhibition appeared

to impede the recovery of Cluster 5 from 2 h after heat shock based on the boundary of the 95% CI (**Fig. 4C**). It also appeared to suppress the gain in insolubility of proteins in Cluster 6. To more specifically identify the proteins that were selectively changed by Hsp70 inhibition during their solubility recovery after heat shock, we performed a Kolmogorov–Smirnov (KS) test to compare their recovery profiles in the presence and absence of Ver155008. This analysis revealed 108 proteins that were significantly impacted (**Table S6**). These proteins were enriched in ribosomal large subunit biogenesis (GO:0042273), regulation of mRNA splicing, via spliceosome (GO:0048024), cytoplasmic translation (GO:0002181) and translational elongation (GO:0006414) (**Fig. 4F**). Therefore, the Hsp70 chaperone network is essential for the solubility recovery of translation, and mRNA splicing upon heat shock.

## CONCLUSION

In this study, we characterized several aspects of the cellular regulatory strategies for recovery from heat shock. First, specific chaperones that form the protein disaggregation machinery are upregulated with a limited fold change during recovery from heat shock. In addition, cytosolic and mitochondrial ribosomal proteins are rapidly down-regulated upon heat shock, which may operate to drive the shutdown of global translation. It is noteworthy that specific ribosomal subunits are most down-regulated. One example is Rpl40, whose down-regulation was previously reported to lead to the specialized ribosome that favors the translation of stress-related proteins[33]. This is consistent with the hypothesis that the specialized ribosome is induced by heat shock to promote the translation of specific chaperones.

Next, compared to only a handful of proteins that underwent abundance changes (19), more than 50% of the proteome changed in solubility either upwards or downwards upon heat shock. These findings support a concept originally proposed in yeast, that the major responses to heat shock in the proteome are in adaptive autoregulatory assembly and disassembly of mature protein complexes and that these changes arise independently to the denaturation of newly synthesized proteins[5]. It is also consistent with a broader context seen in cellular stresses anticipated to affect protein folding quality control[15]. The fast recovery of protein solubility happens within 2 h after heat shock, and coincides with the timepoint where protein levels of ribosomal subunits are returned to pre-heat shock conditions. After 2 h, the recovery of solubility slows down. This might be due to the limited resources available for protein solubility recovery as normal cellular activities start to resume.

Last, our analysis reveals the functional role of Hsp70 in regulating the proteome solubility recovery from heat shock. A previous proteomics study showed that Hsp70 protects a thermal sensitive subproteome in *E. coli*[34]. Our study extends this Hsp70 protective function to the recovery from heat shock, and reveals that Hsp70 also regulates the recovery of the biological condensates formed by many nuclear proteins. These proteins may represent the metastable proteins that are generally protected by Hsp70.

## SUPPORTING INFORMATION

The following supporting information is available free of charge at ACS website [link here].

Table S1 - Total proteomics dataset during recovery from heat shock with and without Hsp70 inhibition

Table S2 - Solubility proteomics dataset during recovery from heat shock with and without Hsp70 inhibition

Table S3 - A list of proteins with their solubility clustered by K-means clustering

Table S4 - Gene Ontology terms associated with the solubility datasets

Table S5 - Raw data of melting temperatures, ΔG of folding and changes in solubility

Table S6 - A list of proteins with their solubility specifically affected by Hsp70 inhibition

Figure S1 - The amount of total proteins loaded on the gels shown in Fig. 1C.

Figure S2 - The abundance changes of non-unique Hsp70 peptides after heat shock and during recovery.

Figure S3 - Protein abundance changes of the components of the proteostasis network.

Figure S4 - Schematic of the proteomics workflow and analysis regarding the solubility (pSup) analysis.

Figure S5 - Comparison of physicochemical properties between soluble proteins and aggregators upon heat shock.

Figure S6 - Supplementary figures showing the data without p-val smoothing for Figs. 2B, 3, 4B, 4C and 5.

## ACKNOWLEDGEMENTS

We thank Professors David B. Ascher, Douglas E. V. Pires (University of Melbourne) and Professor Hongmei Jiang (Northwestern University) for discussions on proteomics data analysis. This work was funded by grants to DMH (National Health and Medical Research Council APP1161803 and to DMH and GER (Australian Research Council DP170103093).

## AUTHOR CONTRIBUTIONS

X.S. designed and performed the experiments, analyzed the data and wrote the manuscript. S.N. helped perform the proteomics experiments. D.C. helped some of the data analysis. G.E.R. oversaw the proteomics experimental design and analysis. D.M.H. oversaw the project, the design of the experiments, interpretation of the data and drafting of the manuscript.

## DECLARATIONS OF INTEREST

The authors declare no competing interests.

## REFERENCES


1. Morimoto, R. I., The heat shock response: systems biology of proteotoxic stress in aging and disease. *Cold Spring Harb Symp Quant Biol* **2011,** *76*, 91-9.

2. Muhlhofer, M.; Berchtold, E.; Stratil, C. G.; Csaba, G.; Kunold, E.; Bach, N. C.; Sieber, S. A.; Haslbeck, M.; Zimmer, R.; Buchner, J., The Heat Shock Response in Yeast Maintains Protein Homeostasis by Chaperoning and Replenishing Proteins. *Cell Rep* **2019,** *29* (13), 4593-4607 e8.

3. Jarnuczak, A. F.; Albornoz, M. G.; Eyers, C. E.; Grant, C. M.; Hubbard, S. J., A quantitative and temporal map of proteostasis during heat shock in Saccharomyces cerevisiae. *Mol Omics* **2018,** *14* (1), 37-52.

4. Woerner, A. C.; Frottin, F.; Hornburg, D.; Feng, L. R.; Meissner, F.; Patra, M.; Tatzelt, J.; Mann, M.; Winklhofer, K. F.; Hartl, F. U.; Hipp, M. S., Cytoplasmic protein aggregates interfere with nucleocytoplasmic transport of protein and RNA. *Science* **2016,** *351* (6269), 173-6.

5. Wallace, E. W.; Kear-Scott, J. L.; Pilipenko, E. V.; Schwartz, M. H.; Laskowski, P. R.; Rojek, A. E.; Katanski, C. D.; Riback, J. A.; Dion, M. F.; Franks, A. M.; Airoldi, E. M.; Pan, T.; Budnik, B. A.; Drummond, D. A., Reversible, Specific, Active Aggregates of Endogenous Proteins Assemble upon Heat Stress. *Cell* **2015,** *162* (6), 1286-98.

6. Buchan, J. R.; Parker, R., Eukaryotic stress granules: the ins and outs of translation. *Mol Cell* **2009,** *36* (6), 932-41.

7. Rosenzweig, R.; Nillegoda, N. B.; Mayer, M. P.; Bukau, B., The Hsp70 chaperone network. *Nature reviews. Molecular cell biology* **2019,** *20* (11), 665-680.

8. Kose, S.; Furuta, M.; Imamoto, N., Hikeshi, a nuclear import carrier for Hsp70s, protects cells from heat shock-induced nuclear damage. *Cell* **2012,** *149* (3), 578-89.

9. Velazquez, J. M.; Lindquist, S., hsp70: nuclear concentration during environmental stress and cytoplasmic storage during recovery. *Cell* **1984,** *36* (3), 655-62.

10. Nillegoda, N. B.; Kirstein, J.; Szlachcic, A.; Berynskyy, M.; Stank, A.; Stengel, F.; Arnsburg, K.; Gao, X.; Scior, A.; Aebersold, R.; Guilbride, D. L.; Wade, R. C.; Morimoto, R. I.; Mayer, M. P.; Bukau, B., Crucial HSP70 co-chaperone complex unlocks metazoan protein disaggregation. *Nature* **2015,** *524* (7564), 247-51.

11. Yoo, H.; Bard, J. A. M.; Pilipenko, E. V.; Drummond, D. A., Chaperones directly and efficiently disperse stress-triggered biomolecular condensates. *Mol Cell* **2022,** *82* (4), 741-755 e11.

12. Maatta, T. A.; Rettel, M.; Sridharan, S.; Helm, D.; Kurzawa, N.; Stein, F.; Savitski, M. M., Aggregation and disaggregation features of the human proteome. *Mol Syst Biol* **2020,** *16* (10), e9500.

13. Maxwell, B. A.; Gwon, Y.; Mishra, A.; Peng, J.; Nakamura, H.; Zhang, K.; Kim, H. J.; Taylor, J. P., Ubiquitination is essential for recovery of cellular activities after heat shock. *Science* **2021,** *372* (6549), eabc3593.

14. Williamson, D. S.; Borgognoni, J.; Clay, A.; Daniels, Z.; Dokurno, P.; Drysdale, M. J.; Foloppe, N.; Francis, G. L.; Graham, C. J.; Howes, R.; Macias, A. T.; Murray, J. B.; Parsons, R.; Shaw, T.; Surgenor, A. E.; Terry, L.; Wang, Y.; Wood, M.; Massey, A. J., Novel adenosine-derived inhibitors of 70 kDa heat shock protein, discovered through structure-based design. *Journal of medicinal chemistry* **2009,** *52* (6), 1510-3.

15. Sui, X.; Pires, D. E. V.; Ormsby, A. R.; Cox, D.; Nie, S.; Vecchi, G.; Vendruscolo, M.; Ascher, D. B.; Reid, G. E.; Hatters, D. M., Widespread remodeling of proteome solubility in response to different protein homeostasis stresses. *Proceedings of the National Academy of Sciences* **2020,** *117* (5), 201912897.

16. Cox, D.; Ang, C.-S.; Nillegoda, N. B.; Reid, G. E.; Hatters, D. M., Hidden information on protein function in censuses of proteome foldedness. *bioRxiv* **2021**, 2021.02.24.432609.

17. Eibe Frank, M. A. H., and Ian H. Witten, The WEKA Workbench. Online Appendix for "Data Mining: Practical Machine Learning Tools and Techniques", Morgan Kaufmann, Fourth Edition. **2016**.

18. Shannon, P.; Markiel, A.; Ozier, O.; Baliga, N. S.; Wang, J. T.; Ramage, D.; Amin, N.; Schwikowski, B.; Ideker, T., Cytoscape: a software environment for integrated models of biomolecular interaction networks. *Genome Res* **2003,** *13* (11), 2498-504.

19. Szklarczyk, D.; Morris, J. H.; Cook, H.; Kuhn, M.; Wyder, S.; Simonovic, M.; Santos, A.; Doncheva, N. T.; Roth, A.; Bork, P.; Jensen, L. J.; von Mering, C., The STRING database in 2017: quality-controlled protein-protein association networks, made broadly accessible. *Nucleic acids research* **2017,** *45* (D1), D362-D368.

20. Cock, P. J.; Antao, T.; Chang, J. T.; Chapman, B. A.; Cox, C. J.; Dalke, A.; Friedberg, I.; Hamelryck, T.; Kauff, F.; Wilczynski, B.; de Hoon, M. J., Biopython: freely available Python tools for computational molecular biology and bioinformatics. *Bioinformatics* **2009,** *25* (11), 1422-3.

21. Erdos, G.; Pajkos, M.; Dosztanyi, Z., IUPred3: prediction of protein disorder enhanced with unambiguous experimental annotation and visualization of evolutionary conservation. *Nucleic acids research* **2021,** *49* (W1), W297-W303.

22. Vizcaino, J. A.; Csordas, A.; del-Toro, N.; Dianes, J. A.; Griss, J.; Lavidas, I.; Mayer, G.; Perez-Riverol, Y.; Reisinger, F.; Ternent, T.; Xu, Q. W.; Wang, R.; Hermjakob, H., 2016 update of the PRIDE database and its related tools. *Nucleic Acids Res* **2016,** *44* (D1), D447-56.

23. DiDomenico, B. J.; Bugaisky, G. E.; Lindquist, S., Heat shock and recovery are mediated by different translational mechanisms. *Proc Natl Acad Sci U S A* **1982,** *79* (20), 6181-5.

24. Crippa, V.; Carra, S.; Rusmini, P.; Sau, D.; Bolzoni, E.; Bendotti, C.; De Biasi, S.; Poletti, A., A role of small heat shock protein B8 (HspB8) in the autophagic removal of misfolded proteins responsible for neurodegenerative diseases. *Autophagy* **2010,** *6* (7), 958-60.

25. Siegert, R.; Leroux, M. R.; Scheufler, C.; Hartl, F. U.; Moarefi, I., Structure of the molecular chaperone prefoldin: unique interaction of multiple coiled coil tentacles with unfolded proteins. *Cell* **2000,** *103* (4), 621-32.

26. Godet, A. C.; David, F.; Hantelys, F.; Tatin, F.; Lacazette, E.; Garmy-Susini, B.; Prats, A. C., IRES Trans-Acting Factors, Key Actors of the Stress Response. *Int J Mol Sci* **2019,** *20* (4), 924.

27. Komar, A. A.; Hatzoglou, M., Cellular IRES-mediated translation: the war of ITAFs in pathophysiological states. *Cell Cycle* **2011,** *10* (2), 229-40.

28. Hundley, H. A.; Walter, W.; Bairstow, S.; Craig, E. A., Human Mpp11 J protein: ribosome-tethered molecular chaperones are ubiquitous. *Science* **2005,** *308* (5724), 1032-4.

29. Bukau, B.; Horwich, A. L., The Hsp70 and Hsp60 chaperone machines. *Cell* **1998,** *92* (3), 351-66.

30. Jarzab, A.; Kurzawa, N.; Hopf, T.; Moerch, M.; Zecha, J.; Leijten, N.; Bian, Y.; Musiol, E.; Maschberger, M.; Stoehr, G.; Becher, I.; Daly, C.; Samaras, P.; Mergner, J.; Spanier, B.; Angelov, A.; Werner, T.; Bantscheff, M.; Wilhelm, M.; Klingenspor, M.; Lemeer, S.; Liebl, W.; Hahne, H.; Savitski, M. M.; Kuster, B., Meltome atlas-thermal proteome stability across the tree of life. *Nat Methods* **2020**, *17* (5), 495-503.

31. Walker, E. J.; Bettinger, J. Q.; Welle, K. A.; Hryhorenko, J. R.; Ghaemmaghami, S., Global analysis of methionine oxidation provides a census of folding stabilities for the human proteome. *Proc Natl Acad Sci U S A* **2019,** *116* (13), 6081-6090.

32. Schlecht, R.; Scholz, S. R.; Dahmen, H.; Wegener, A.; Sirrenberg, C.; Musil, D.; Bomke, J.; Eggenweiler, H. M.; Mayer, M. P.; Bukau, B., Functional analysis of Hsp70 inhibitors. *Plos One* **2013,** *8* (11), e78443.

33. Lee, A. S.; Burdeinick-Kerr, R.; Whelan, S. P., A ribosome-specialized translation initiation pathway is required for cap-dependent translation of vesicular stomatitis virus mRNAs. *Proc Natl Acad Sci U S A* **2013,** *110* (1), 324-9.

34. Zhao, L.; Vecchi, G.; Vendruscolo, M.; Korner, R.; Hayer-Hartl, M.; Hartl, F. U., The Hsp70 Chaperone System Stabilizes a Thermo-sensitive Subproteome in E. coli. *Cell Rep* **2019,** *28* (5), 1335-1345 e6.

For TOC Only

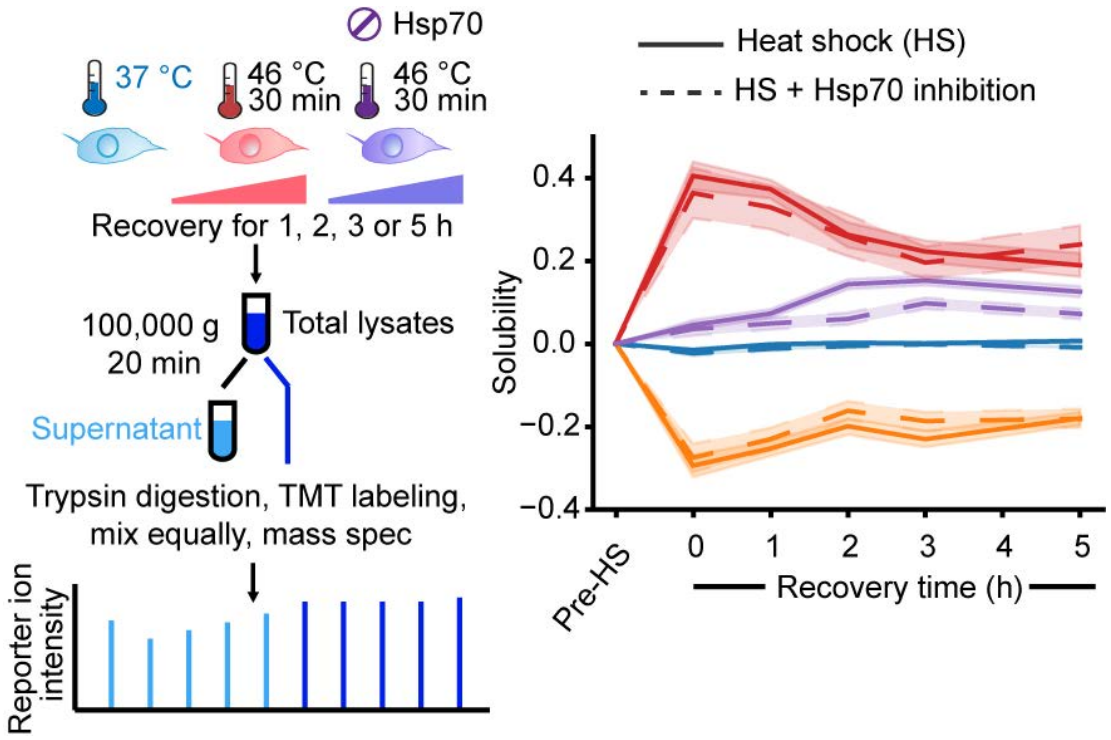


All images used in the TOC graphic is original, 100% created by authors ONLY, and not been published elsewhere.